# Electronic structure and magneto-optical Kerr effect spectra of ferromagnetic shape-memory Ni-Mn-Ga alloys: Experiment and density functional theory calculations

S. Uba, A. Bonda, and L. Uba
*Faculty of Mathematics and Informatics, University of Bialystok, K. Ciolkowskiego 1M, PL-15-245 Bialystok, Poland*

L. V. Bekenov and V. N. Antonov
*Institute of Metal Physics, Vernadsky Street, 03142 Kiev, Ukraine*

A. Ernst
*Max-Planck Institut für Mikrostrukturphysik, Weinberg 2, D-06120 Halle, Germany*
(Received 4 March 2016; revised manuscript received 10 August 2016; published 25 August 2016)

In this joint experimental and *ab initio* study, we focused on the influence of the chemical composition and martensite phase transition on the electronic, magnetic, optical, and magneto-optical properties of the ferromagnetic shape-memory Ni-Mn-Ga alloys. The polar magneto-optical Kerr effect (MOKE) spectra for the polycrystalline sample of the Ni-Mn-Ga alloy of $Ni_{60}Mn_{13}Ga_{27}$ composition were measured by means of the polarization modulation method over the photon energy range $0.8 \leqslant h\nu \leqslant 5.8$ eV in magnetic field up to 1.5 T. The optical properties (refractive index $n$ and extinction coefficient $k$) were measured directly by spectroscopic ellipsometry using the rotating analyzer method. To complement experiments, extensive first-principles calculations were made with two different first-principles approaches combining the advantages of a multiple scattering Green function method and a spin-polarized fully relativistic linear-muffin-tin-orbital method. The electronic, magnetic, and MO properties of Ni-Mn-Ga Heusler alloys were investigated for the cubic austenitic and modulated 7M-like incommensurate martensitic phases in the stoichiometric and off-stoichiometric compositions. The optical and MOKE properties of Ni-Mn-Ga systems are very sensitive to the deviation from the stoichiometry. It was shown that the *ab initio* calculations reproduce well experimental spectra and allow us to explain the microscopic origin of the $Ni_2MnGa$ optical and magneto-optical response in terms of interband transitions. The band-by-band decomposition of the $Ni_2MnGa$ MOKE spectra is presented and the interband transitions responsible for the prominent structures in the spectra are identified.

DOI: 10.1103/PhysRevB.94.054427

## I. INTRODUCTION

Ferromagnetic shape-memory alloys displaying large magnetic-field-induced strain (MFIS) have recently emerged as a class of active materials, very promising for actuator and sensor applications. The interest in ferromagnetic shape memory compounds stems from the possibility to control the phase transition by application of a magnetic field [1]. The response of the system to a field is faster than that obtained by changing temperature or applying stress, thus substantially increasing the range of applications. The stoichiometric $Ni_2MnGa$ is a ferromagnetic material exhibiting a martensitic transition from a high-temperature Heusler austenitic structure to a related tetragonal form with a 6.6% $c$ axis contraction at the martensitic transformation temperature ($T_M$) equal to 202 K [2,3]. Associated with this phase transition the material exhibits shape memory properties enabling the system to reverse large deformations in the martensitic phase by heating into the cubic phase. The stoichiometric $Ni_2MnGa$ is the most investigated compound as it shows not only extremely large MFIS [4,5] but also a large magnetocaloric effect [6] and negative magnetoresistance [7], which are very useful for technological applications.

Since Ullakko *et al.* [3] discovered large MFIS in a Heusler alloy $Ni_2MnGa$ single crystal in 1996, numerous theoretical and experimental works on $Ni_2MnGa$ were published [8–36]. It was shown that basic structural, elastic, and magnetic properties, such as magnetic moments, magnetic anisotropy energy, the equilibrium structure, elastic constants, etc. of $Ni_2MnGa$ alloy both in austenitic and martensitic phases can be reproduced in *ab initio* calculations with fairly high accuracy [9–11,15,19,20,23,27–32].

It was discovered recently that the magnetic and structural transitions take place not only in the stoichiometric alloy but also in alloys with significant deviations from stoichiometry [4,5]. It was found that the values of $T_M$ and Curie temperature ($T_C$) vary strongly with the composition. Murray *et al.* [4] reported large MFIS of 6% in a ferromagnetic martensitic $Ni_{49.8}Mn_{28.5}Ga_{21.7}$ alloy at room temperature. Sozinov *et al.* [5] declared $Ni_{48.8}Mn_{29.7}Ga_{21.5}$ orthorhombic 7M martensitic that they acquired giant MFIS of ∼9.5% in the phase. Wang *et al.* [37] obtained large reversible MFIS of −0.6 % in the $Ni_{53}Mn_{22}Ga_{25}$ single crystal at 300 K.

The dope composition strongly influences the electronic, structural, and magnetic properties of Ni-Mn-Ga shape memory alloys [21,36,38–41]. Chakrabarti *et al.* [21] show that the total magnetic moment decreases with Ni excess. Therewith, an Ni doping decreases the unit cell volume, whereas an Mn doping increases it [36]. Jiang *et al.* [42] demonstrated experimentally that the measured high-field saturation magnetization is equal to 4.38 $\mu_B$ and 2.93 $\mu_B$ in $Ni_{50}Mn_{25}Ga_{25}$ and $Ni_{50}Mn_{30}Ga_{20}$ alloys, respectively. The martensitic transformation start temperatures enhance monotonically from 283.9 K for $Ni_{50}Mn_{27}$ $Ga_{23}$ to 375.9 K for $Ni_{50}Mn_{30}$ $Ga_{20}$. The martensitic transformation temperature

 

$T_M$ increases from 202 K to 315 K and 350 K if the composition is changed from the stoichiometric one to $Ni_{54}Mn_{21}Ga_{20}$ and $Ni_{50}Mn_{28}Ga_{22}$, respectively [41].

The microscopic origin of the martensitic transition remains under debate. The main proposals were the band Jahn-Teller mechanism [8,20] or strong electron phonon-coupling and Fermi surface (FS) nesting [43]. The latter has been supported by extended *ab initio* calculations [12,16,17]. Shapiro *et al.* [44] using neutron scattering experiments found well-defined phason excitations, which were associated to the charge density wave (CDW) resulting from FS nesting. Furthermore, ultraviolet photoemission measurements have shown the formation of a pseudogap 0.3 eV below the Fermi energy at $T_M$ [45], which has also been attributed to CDW due to the FS nesting.

Magneto-optical (MO) spectroscopy in combination with spectroscopic ellipsometry has a great advantage in the investigation of the electronic structure of MFIS materials in comparison with other methods. The MO spectroscopy is very sensitive to the crystal structure and chemical composition [46], valence phase transitions [47], as well as induced strain [48], crystallographic orientation [49], and magnetization direction [50]. Despite many experimental and theoretical studies of electronic and magnetic structures of $Ni_2MnGa$ compounds, there are quite a few publications devoted to optical and MO Kerr effect (MOKE) spectra of $Ni_2MnGa$ [51–57]. Kudryavtsev with co-workers [52–54] measured the MO Kerr effect in a stoichiometric polycrystalline $Ni_2MnGa$ alloy but only in the equatorial geometry, which is very sensitive to the angle of incidence. Park [55] measured the magneto-optical Kerr effect for ferromagnetic $Ni_2MnGa$ at room temperature with nearly normal-incident polar geometry for the (100), (110), and (111) sample planes and for martensite phase at 100 K for (100) plane. Also optical and magneto-optical spectra of cubic austenite phase of $Ni_2MnGa$ were calculated with the TB-LMTO method by the same author [55]. Recently Beran *et al.* [56,57] studied optical and MOKE properties in the polar geometry of a single $Ni_{50.1}Mn_{28.4}Ga_{21.5}$ crystal during the transformation from the austenitic phase into the modulated 10M martensitic phase. They showed that MO spectra of polar Kerr rotation exhibited significant changes by crossing the transformation temperature.

In $Ni_2MnGa$ compounds, we have a situation where the interplay between an incommensurate structural modulation, a splitting of the electronic states due to the tetragonal or orthorhombic distortion of the cubic lattice and the ferromagnetic order, combine to stabilize a phase displaying a large magnetic shape-memory effect. To guide the rational design of the MFIS materials the microscopic origin of their functional properties must be understood, which requires methods that can disentangle the interplay between electronic, magnetic, and structural degrees of freedom.

The aim of the present paper is to investigate the capability of the theoretical calculations to adequately predict from first principles the influence of the chemical composition and martensitic phase transition effects on electronic, magnetic, optical, and magneto-optical properties of Ni-Mn-Ga Heusler alloys. Probing various functionals within the modern density functional theory we have shown that all the above mentioned properties could be correctly obtained with a conventional GGA approach. We obtain an excellent agreement between the calculated and experimentally measured ground state properties (equilibrium lattice parameters), magnetic critical phenomena (exchange parameters and Curie temperature), as well as excited state properties (optical and MO) of $Ni_2MnGa$ for austenite and martensite phases.

This paper is organized as follows. Section II presents a description of the crystal structure for high-temperature and low-temperature phases of the $Ni_2MnGa$ Heusler alloy and the computational and experimental details. Section III is devoted to experimental measurements of the optical and MO Kerr spectra and theoretical calculations of the electronic structure and MOKE spectra of $Ni_2MnGa$ using the fully relativistic Dirac LMTO band structure method. Theoretically calculated spectra are compared with experimentally measured spectra. Finally, the results are summarized in Sec. IV.

## II. CRYSTAL STRUCTURE, COMPUTATIONAL AND EXPERIMENTAL DETAILS

### A. Crystal structure

The Heusler-type $Ni_2MnGa$ compound crystallizes at high temperatures in the cubic $L2_1$ structure with $Fm\bar{3}m$ symmetry (No. 225), which is formed by four interpenetrating fcc sublattices [Fig. 1(a)]. The Ni ions occupy the 4*b* Wyckoff positions ($x = \frac{1}{4}$, $y = \frac{1}{4}$, $z = \frac{1}{4}$). The Mn ions occupy the 4*a* positions ($x = 0$, $y = 0$, $z = 0$) and the Ga ions are placed at the 4*b* sites ($x = \frac{1}{2}$, $y = \frac{1}{2}$, $z = \frac{1}{2}$). Both the Ni and Mn atoms have eight nearest neighbors at the same distance. Mn has eight Ni atoms as nearest neighbors, while for Ni there are four Mn and four Ga atoms. At room temperature (RT), it is ferromagnetic and the Curie temperature is slightly higher than RT, $T_C \sim 376$ K.

Upon cooling of the alloy, the high-temperature cubic phase passes into a quasicubic modulated phase 3M at premartensitic transition temperature $T_{PM} = 260$ K with a modulation period equal to six atomic planes. Upon further cooling of the alloy, there occurs a structural transition from the quasicubic phase 3M into the modulated martensitic phase at the martensitic transformation temperature $T_M$ [2,40,58].

The structure of the low-temperature martensitic phase of $Ni_2MnGa$ has been extensively investigated using different diffraction techniques; however, the actual martensitic crystal structure is still controversial [40,58,59]. The martensitic phase has been described as a nearly tetragonal [2] or orthorhombic [60] distortion of the parent cubic phase with an additional long-wavelength modulation along the *c* axis. Webster *et al.* [2] studied the martensitic structure of $Ni_2MnGa$ using neutron powder diffraction measurements and reported a tetragonal *bct* structure. Martynov reported a five-layer modulated martensitic structure on the basis of single-crystal x-ray diffraction data [61]. Brown *et al.* [60] and Ranjan *et al.* [62] showed that the structure of the martensitic phase is orthorhombic with 7M commensurate modulation. However, several authors have reported that the modulated phase of $Ni_2MnGa$ possesses an incommensurate structure. Righi *et al.* [63] reported incommensurate modulation of 5M type with the modulation vector $\mathbf{q} = (2/5 + \delta)\mathbf{c}^*$ where the incommensuration parameter $\delta = 0.0248$. However, subsequent

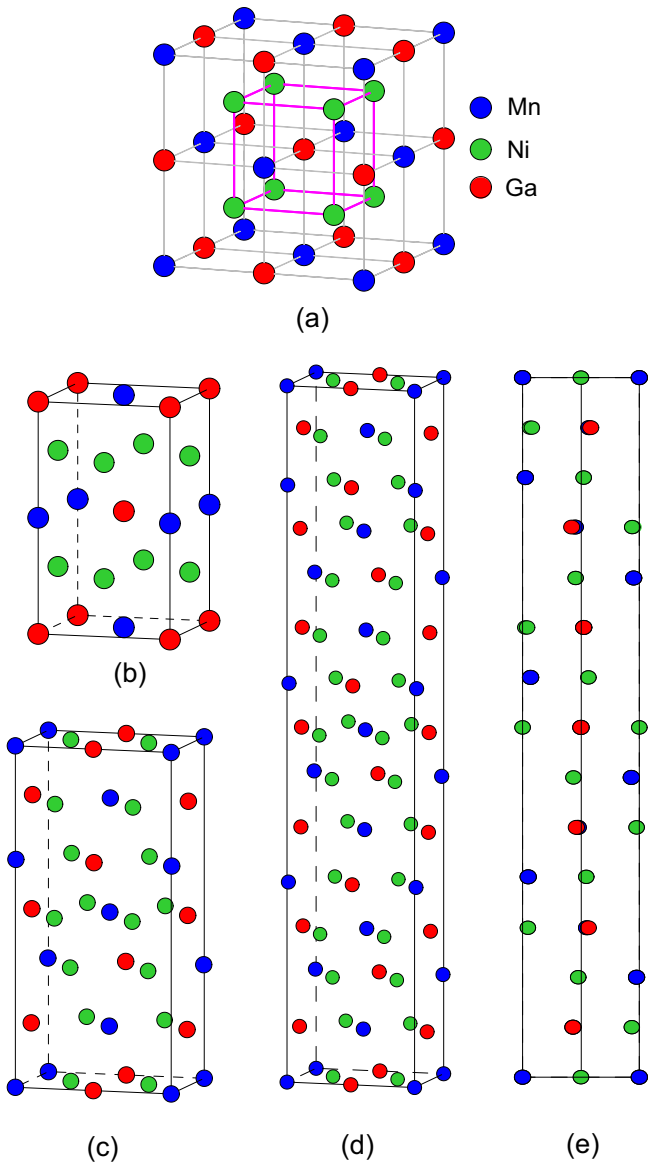


FIG. 1. Schematic representation of the crystal structure of $Ni_2MnGa$ alloy: (a) a high-temperature austenitic phase with a cubic lattice of $L2_1$ type (contains four primitive cells); (b) a body centered tetragonal ($bct$) martensitic phase of $L1_0$ type; (c) the 3M premartensitic structure of $Pnmn$ orthorhombic type; (d) the martensitic 7M superstructure of $Immm$ orthorhombic type (e) modulated orthorhombic unite cell of $Ni_2MnGa$ martensite phase projected in the $a$-$c$ plane highlighting the atomic position modulation in its rational approximant 7M structure.

single-crystal diffraction studies of Fukuda *et al.* [64] have revealed that the incommensurate phase might be of a 7M-type for the stoichiometric $Ni_2MnGa$ composition. Singh *et al.* [58] also rejects the 5M-like rational approximant structure of the martensitic phase and confirms the 7M-like incommensurate modulation of the martensitic phase with the orthorhombic $Immm$ space group with the modulation wave vector $\mathbf{q} = (3/7 + \delta)\mathbf{c}^*$ where the incommensuration parameter $\delta = 0.00303$. Finally, we should remark that some of these structural differences may originate in sample preparation details and can be sensitive to stoichiometry [65]. Figure 1 shows schematic representations of different crystal structures of $Ni_2MnGa$ alloy.

### B. Computational details

MO effects refer to various changes in the polarization state of light upon interaction with materials possessing a net magnetic moment, including rotation of the plane of linearly polarized light (Faraday, Kerr rotation), and the complementary differential absorption of left and right circularly polarized light (circular dichroism). In the near visible spectral range these effects result from excitation of electrons in the conduction band. Near x-ray absorption edges, or resonances, MO effects can be enhanced by transitions from well-defined atomic core levels to selected valence states. Using straightforward symmetry considerations it can be shown that all MO phenomena are caused by the symmetry reduction, in comparison to the paramagnetic state, caused by magnetic ordering [66]. Concerning optical properties this symmetry reduction only has consequences when SO coupling is considered in addition. To calculate MO properties one therefore has to account for magnetism and SO coupling at the same time when dealing with the electronic structure of the material considered.

For the polar Kerr magnetization geometry and a crystal of orthorhombic symmetry, where both the $c$ axis and the magnetization $\mathbf{M}$ are perpendicular to the sample surface and the $z$ axis is chosen to be parallel to them, the dielectric tensor is composed of the diagonal $\varepsilon_{xx}$, $\varepsilon_{yy}$, and $\varepsilon_{zz}$, and the off-diagonal $\varepsilon_{xy}$ component in the form

$$\boldsymbol{\varepsilon} = \begin{pmatrix} \varepsilon_{xx} & \varepsilon_{xy} & 0 \\ -\varepsilon_{xy} & \varepsilon_{yy} & 0 \\ 0 & 0 & \varepsilon_{zz} \end{pmatrix}. \tag{1}$$

The various elements $\hat{\varepsilon}_{\alpha\beta}$ are composed of real and imaginary parts as follows: $\varepsilon_{\alpha\beta} = \varepsilon^{(1)}_{\alpha\beta} + i\varepsilon^{(2)}_{\alpha\beta}$. The diagonal elements, $\varepsilon_{xx}$, $\varepsilon_{yy}$, and $\varepsilon_{zz}$ are squares of the complex refractive indexes $N = (n + ik)$, where $n$ and $k$ are refractive index and extinction coefficient, respectively, for the corresponding axis. The optical conductivity tensor $\hat{\sigma}_{\alpha\beta} = \sigma^{(1)}_{\alpha\beta} + i\sigma^{(2)}_{\alpha\beta}$ is related to the dielectric tensor $\varepsilon_{\alpha\beta}$ through the equation

$$\hat{\varepsilon}_{\alpha\beta}(\omega) = \delta_{\alpha\beta} + \frac{4\pi i}{\omega}\hat{\sigma}_{\alpha\beta}(\omega). \tag{2}$$

For an orthorhombic crystal and magnetic field oriented along the $c$ axis, the complex polar Kerr angle at the normal incidence, $\theta + i\eta$, is described by the expression [67–69]

$$\theta + i\eta \approx \frac{-\varepsilon_{xy}}{(\varepsilon_0 - 1)\sqrt{\varepsilon_0}}, \tag{3}$$

where $\theta$ and $\eta$ is the Kerr rotation and ellipticity, respectively, and $\varepsilon_0 = (\varepsilon_{xx} + \varepsilon_{yy})/2$. In an orthorhombic crystal for the quasitetragonal case, $\varepsilon_{xx} \approx \varepsilon_{yy}$, and $\varepsilon_0 \approx \varepsilon_{xx}$. Therefore, in the following, we will use the symbols $\varepsilon_{xx}$ and $\sigma_{xx}$ for designation of the diagonal elements of the dielectric tensor and optical conductivity.

The optical conductivity of $Ni_2MnGa$ has been computed from the energy band structure by means of the

Kubo-Greenwood [70] linear-response expression [71]:

$$\sigma_{\alpha\beta}(\omega) = \frac{-ie^2}{m^2\hbar V_{uc}} \sum_{\mathbf{k}} \sum_{nn'} \times \frac{f(\epsilon_{n\mathbf{k}}) - f(\epsilon_{n'\mathbf{k}})}{\omega_{nn'}(\mathbf{k})} \frac{\Pi^{\alpha}_{n'n}(\mathbf{k})\Pi^{\beta}_{nn'}(\mathbf{k})}{\omega - \omega_{nn'}(\mathbf{k}) + i\gamma}, \quad (4)$$

where $f(\epsilon_{n\mathbf{k}})$ is the Fermi function, $\hbar\omega_{nn'}(\mathbf{k}) \equiv \epsilon_{n\mathbf{k}} - \epsilon_{n'\mathbf{k}}$ is the energy difference of the Kohn-Sham energies, and $\gamma$ is the lifetime parameter, which is included to describe the finite lifetime of the excited Bloch electron states. The $\Pi^{\alpha}_{nn'}$ are the dipole optical transition matrix elements, which in a fully relativistic description are given by

$$\mathbf{\Pi}_{nn'}(\mathbf{k}) = m\langle\psi_{n\mathbf{k}}|c\boldsymbol{\alpha}|\psi_{n'\mathbf{k}}\rangle \quad (5)$$

with $\psi_{n\mathbf{k}}$ being the four-component Bloch electron wave function. The combined correction terms were also taken into account in the optical matrix element calculations. The detailed description of the optical matrix elements in the Dirac representation is given in Ref. [72]. We should mention, lastly, that the absorptive part of the optical conductivity was calculated in a wide energy range and then the Kramers-Kronig transformation was used to calculate the dispersive parts of the optical conductivity from the absorptive ones.

The details of the computational method are described in our previous papers [50,73,74], and here we only mention several aspects. The calculations were performed using the spin-polarized fully relativistic linear-muffin-tin-orbital (SPR LMTO) method [75,76] in the atomic sphere approximation (ASA) with the combined correction term taken into account. The exchange-correlation functional of a GGA-type was used in the version of Perdew, Burke, and Ernzerhof (PBE) [77,78]. Brillouin zone (BZ) integrations were performed using the improved tetrahedron method [79]. The basis consisted of transition metal $s$, $p$, $d$, and $f$, and Ga $s$, $p$, and $d$ LMTO's. We performed the calculations for the structures studied varying lattice parameters and determining the minima of total energies for Brillouin zone divisions ensuring required accuracies, up to $30 \times 30 \times 30$ Brillouin zone division. The estimated equilibrium lattice parameters corresponding to the minima of the total energy were then compared with the available experimental structural data and used in further calculations.

The austenitic high temperature Heusler structure possesses a cubic symmetry of space group $Fm\bar{3}m$ (No. 225) [2]. For the martensitic phase we used a tetragonal $bct$ structure of $P4/mmm$ symmetry (No. 123) [2] and the 7M-like incommensurate modulated martensitic phase in the orthorhombic $Immm$ space group (No. 71) with the modulation wave vector $\mathbf{q} = (3/7 + \delta)\mathbf{c}^*$ where the incommensuration parameter $\delta = 0.00303$ [58]. Our measurements of the MOKE spectra were carried out on the sample of $Ni_{60}Mn_{13}Ga_{27}$ composition. To calculate the electronic structure and MOKE spectra in Ni-rich alloys in the 7M incommensurate modulated orthorhombic $Immm$ structure, we modified the lattice constants according to Ref. [36] ($a = 4.243$ Å, $b = 5.421$ Å, and $c = 29.317$ Å).

The calculations of the electronic structure and MO properties of nonstoichiometric $Ni_{2+x}Mn_{1\pm y}Ga_{1\pm z}$ alloys were carried out for the $2a \times 2b \times 1c$ and $1a \times 1b \times 4c$ supercells for the $Fm\bar{3}m$, $P4/mmm$, and $Immm$ unit cells for different compositions $x$, $y$ and $z$.

TABLE I. Wyckoff positions $(x,y,z)$ for 7M commensurate modulated orthorhombic structure of the martensite phase of $Ni_2MnGa$ [58].

| Atom | site | $x$ | $y$ | $z$ |
|---|---|---|---|---|
| $Ni_1$ | $4f$ | 0.5 | 0.247 | 0 |
| $Ni_2$ | $8h$ | 0.523 | 0.248 | 0.1429 |
| $Ni_3$ | $8h$ | 0.454 | 0.251 | 0.286 |
| $Ni_4$ | $8h$ | 0.564 | 0.253 | 0.429 |
| $Mn_1$ | $2b$ | 0 | 0 | 0 |
| $Mn_2$ | $4g$ | 0.028 | 0 | 0.1429 |
| $Mn_3$ | $4g$ | 0.948 | 0 | 0.286 |
| $Mn_4$ | $4g$ | 0.056 | 0 | 0.429 |
| $Ga_1$ | $2a$ | 0 | 0.5 | 0 |
| $Ga_2$ | $4g$ | 0.023 | 0.5 | 0.143 |
| $Ga_3$ | $4g$ | 0.951 | 0.5 | 0.286 |
| $Ga_4$ | $4g$ | 0.068 | 0.5 | 0.428 |

The results of calculations for the austenite $L2_1$ structure and 7M modulated commensurate for rational approximant structure with atomic positions listed in Table I are presented in Table II. It is seen that the GGA approach gives the theoretically calculated lattice constants in excellent agreement with the experimental data: the deviation is less than 0.2% for austenite phase and 0.4% for martensite 7M phase (the local spin density was able to produce the deviation for the lattice constants up to 3%). Therefore all the calculations of the optical and MO properties of $Ni_2MnGa$ were carried out with the theoretically obtained lattice constants presented in Table II.

To check the validity of the GGA for studied systems we calculated Curie temperature for the compounds using Heisenberg exchange parameters obtained within the magnetic force theorem as it is implemented within the multiple scattering theory [80]. $T_C$ was estimated within the random phase approximation [81], which provides an adequate description of magnetic critical phenomena. Thereby, we tried several density functional approaches: local spin density approximation (LSDA), GGA, and the LSDA+$U$ method [82]. As result, we found that the GGA method provides the best agreement with experiment ($T_C^{GGA} = 360$ K vs $T_C^{\exp} = 376$ K

TABLE II. Calculated equilibrium lattice constants (in Å), total magnetic moments $M_t$ (in $\mu_B$/f.u.), and Curie temperature $T_C$ (in K) of the austenite $L2_1$ and martensite 7M structures of the $Ni_2MnGa$ compound as compared to experimental data.

| | method | $a$ | $b$ | $c$ | $M_t$ | $T_C$ |
|---|---|---|---|---|---|---|
| austenite | theory | 5.8135 | | | 4.016 | 360 |
| | expr.[a] | 5.825 | | | 4.17 | 376 |
| martensite | theory | 4.2162 | 5.5690 | 29.3010 | 4.105 | |
| | expr.[b] | 4.2186 | 5.5469 | 29.3134 | | |
| | expr.[c] | | | | 3.8 | |
| | expr.[d] | | | | 4.1 | |

[a]Reference [2].
[b]Reference [58].
[c]Reference [83].
[d]Reference [37].

for the cubic $L2_1$ phase), while the LSDA and the LSDA+$U$ approaches underestimate it by 40–100 K dependent on the value of $U$. We think that it is a crucial test since the value of $T_C$ is mainly calculated from exchange constants, which can be interpreted as the wave function overlap integrals. Our calculations show that only the GGA provides a proper description of the electronic states in the studied compounds.

In Table II, total magnetic moments per formula unit for the structures, obtained for the calculated equilibrium lattice constants, are shown as well. It is seen that for the austenite the calculated moment is slightly underestimated, but for the martensite it is overestimated or coincides with the experimental data depending on the particular sample preparation conditions and crystal quality.

### C. Experimental details

The optical and magneto-optical Kerr rotation and ellipticity (MOKE) spectra have been investigated for the polycrystalline sample of the Ni-Mn-Ga alloy of $Ni_{60}Mn_{13}Ga_{27}$ composition prepared by arc melting technique. After melting, the sample was subjected to homogenization by thermal annealing at 1150 K for 70 hours in argon atmosphere. The chemical composition of the sample was determined from x-ray fluorescence analysis, and the alloy remains in martensitic state at room temperature. For the present measurements the sample surface was polished mechanically and subsequently chemically etched to remove the surface contamination introduced by mechanical treatment. The polar MOKE spectra were measured by means of the polarization modulation method using a piezobirefringent modulator. The spectra were measured at room temperature over the photon energy range $0.8 \leqslant h\nu \leqslant 5.8$ eV under saturation condition deduced from the measured hysteresis loop in magnetic field up to 1.5 T. The optical properties—refractive index $n$ and extinction coefficient $k$—were measured directly by spectroscopic ellipsometry using the rotating analyzer method over the same spectral range as MOKE spectra. A detailed description of the MOKE spectrometer and ellipsometer system used is given in Ref. [73]. Both the diagonal and off-diagonal components of the dielectric tensor of the material were determined from the measured MOKE and optical spectra with the use of Eqs. (2) and (3).

## III. RESULTS AND DISCUSSION

### A. Energy band structure

The modulation on the nanoscale and other modifications such as deviation from the stoichiometry of the $Ni_2MnGa$ crystal makes the analysis of the electronic structure of martensite very complex. To obtain a relevant starting point, one has to begin with the parent phase, i.e., austenitic, which is cubic. Additionally, a prerequisite for the magnetic shape memory effect is the martensitic transformation, and thus the knowledge of the precise character of the austenitic phase and its evolution just above the transformation is crucial. Therefore we start with consideration of the electronic structure of the austenitic cubic phase.

The spin-polarized partial densities of states (DOS) of $Ni_2MnGa$ for the austenitic high-temperature $Fm\bar{3}m$ structure

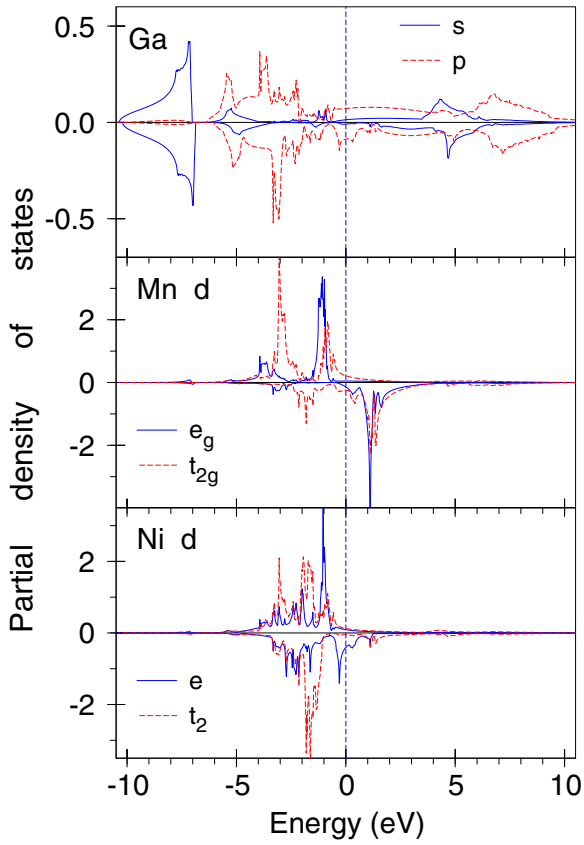


FIG. 2. The symmetry separated GGA partial density of states [in states/(atom eV)] of $Ni_2MnGa$ for the high-temperature $Fm\bar{3}m$ structure.

obtained from fully relativistic GGA calculations are presented in Fig. 2. The results agree well with previous band structure calculations [8–11,19,21,23,55]. The occupied part of the valence band can be subdivided into several regions. The Ga 4$s$ bands appear between −10.3 and −6.8 eV. The next six energy bands in the energy region −6.2 to −3.2 eV are the Ga 4$p$ bands. The Ni and Mn $d$ energy bands are located above and below $E_F$ at about −4.2 to 3.0 eV.

Because of a strong Ga $p$–$p$ hybridization the Ga $p$ states are split into bonding and antibonding states. The former are located between approximately −6.2 and −1 eV, while the latter are spread over a broad energy range above −1 eV. The crystal field at the Mn 4$a$ site ($O_h$ point symmetry) splits the Mn $d$ states into $e_g$ ($3z^2 - 1$ and $x^2 - y^2$) and $t_{2g}$ ($xy$, $yz$, and $xz$) ones. The $t_{2g}$ states are strongly hybridized with the Ga $p$ states and give a significant contribution to the bonding states below −1 eV. The $e_g$ states form weaker Mn $d$–Ga $p$ bonds but they hybridize strongly the $d$ states of eight Ni nearest neighbors.

The center of Ni 3$d$ states ($\varepsilon_v = -1.72$ eV) is found in a gap between the bonding and antibonding Ga $p$ states. The crystal field at the Ni 4$b$ site ($T_d$ point symmetry) causes the splitting of $d$ orbitals into a doublet $e$ ($3z^2 - 1$ and $x^2 - y^2$) and a triplet $t_2$ ($xy$, $yz$, and $xz$). The hybridization between Ni $t_2$ and Mn $t_{2g}$ states splits the Mn spin-down $t_{2g}$ states into two peaks, the bonding one located at ∼1.9 eV below the Fermi level and the unoccupied antibonding peak centered at 1.2 eV.

The Ni $e$ orbitals hybridize weakly Ga $p$ states, however, they hybridize strongly Mn $e_g$ orbitals at around $-1$ eV for the spin-up channel.

In addition to the crystal field splitting, the $3d$ levels of the Ni and Mn atoms are split due to the exchange interaction. The exchange splitting between the spin-up and -down $3d$ electrons on the Ni atom is about 0.5 eV. The corresponding splitting on the Mn atom is much larger, about 2 eV. Spin-orbit splitting of the $3d$ energy bands for both the Ni and Mn atoms is much smaller than their spin and crystal-field splittings. The spin-polarized calculations show that $Ni_2MnGa$ in the high-temperature phase is not a half-metallic ferromagnet. The Fermi level crosses both the majority and minority spin energy bands.

Because nearly all the $3d$ Ni states are occupied (in contrast to the $3d$ Mn states), the main contribution to the total magnetic moment of the alloy (4.02 $\mu_B$) comes from the Mn atoms (3.526 $\mu_B$) while the magnetic moments of the Ni and Ga atoms are rather small (i.e., 0.290 and $-0.080$ $\mu_B$, respectively). The orbital magnetic moments are equal to 0.022, 0.026, and $-0.001$ $\mu_B$ for Ni, Mn, and Ga atoms, respectively in the GGA approximation.

Figure 3 shows the total and partial DOSs of $Ni_2MnGa$ for the 7M-like incommensurate modulated martensitic phase with the orthorhombic $Immm$ space group structure calculated in the fully relativistic spin-polarized approximation. The total magnetic moment of the alloy is increased up to 4.105 $\mu_B$ in the martensitic orthorhombic structure in comparison with the austenitic structure. The averaged spin moments at the Ni sites ($M_s^{Ni} = 0.335$ $\mu_B$) are increased in comparison with the austenitic structure. The moment at the Ga sites is changed insignificantly. The orbital magnetic moments are equal to 0.025 $\mu_B$, 0.027 $\mu_B$, and $-0.001$ $\mu_B$ for Ni, Mn, and Ga atoms, respectively, in the $Immm$ martensitic structure.

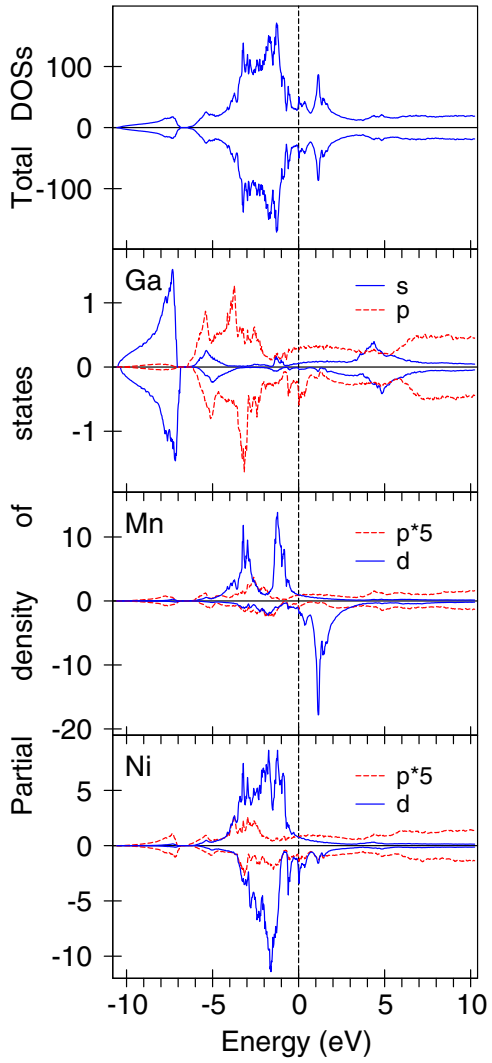


FIG. 3. The total [in states/(cell eV)] and partial [in states/(atom eV)] DOSs of $Ni_2MnGa$ for the 7M-like incommensurate modulated martensitic phase with the orthorhombic $Immm$ space group structure.

### B. Optical and MOKE spectra

Figure 4 shows experimentally measured [53] diagonal optical conductivity (OC) $\sigma_{1xx}$ spectra of $Ni_2MnGa$ for the austenitic (upper panel) and martensitic (lower panel) phases and the spectra calculated by the SPR LMTO method in the GGA approximation. In the following, $\sigma_{1xx}$ and $\sigma_{2xy}$ denote the absorptive parts of the complex diagonal and

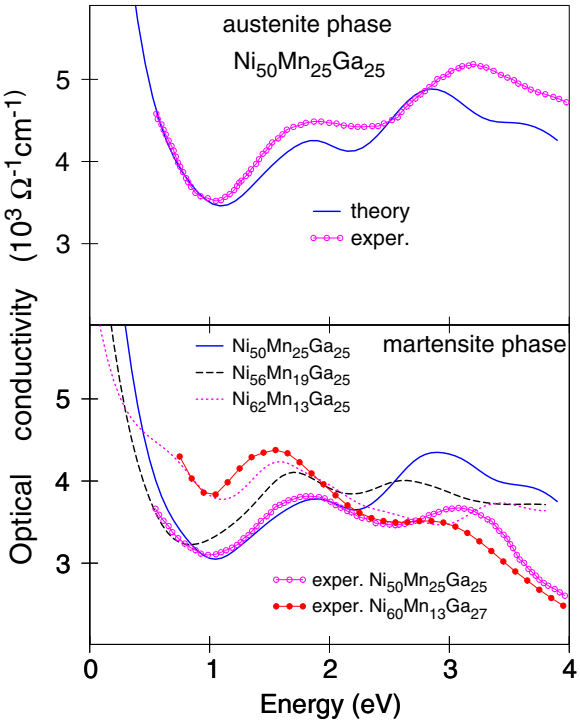


FIG. 4. Upper panel: comparison between experimental diagonal optical conductivity $\sigma_{1xx}$ spectra (open magenta circles) of $Ni_2MnGa$ (Ref. [53]) and the spectra calculated for austenitic $Fm\bar{3}m$ cubic structure (full line) approximation. Lower panel: comparison of the experimental diagonal optical conductivity spectra for a low temperature stoichiometric $Ni_2MnGa$ alloy (open magenta) from Ref. [53] and our measurements in a Ni-rich $Ni_{60}Mn_{13}Ga_{27}$ alloy (closed red circles) in the martensitic phase with the theoretically calculated spectra for stoichiometric (full blue curve), Ni-rich $Ni_{56}Mn_{19}Ga_{25}$ (dashed black curve) and $Ni_{62}Mn_{13}Ga_{25}$ (dotted magenta curve) alloys of the low-temperature $Immm$ orthorhombic type.

off-diagonal optical conductivities $\sigma_{xx} = \sigma_{1xx} + i\sigma_{2xx}$ and $\sigma_{xy} = \sigma_{1xy} + i\sigma_{2xy}$, respectively. The experimental optical conductivity spectrum $\sigma_{1xx}$ has a low energy minimum at around 1.0 eV and two maxima at 1.7 eV and 3.2 eV. The GGA calculations give reasonable agreement in the energy position of the minimum and low energy maximum, however, the high energy peak is slightly shifted towards lower energy.

The lower panel of Fig. 4 presents the comparison of the experimental diagonal optical conductivity spectra for a martensitic stoichiometric $Ni_2MnGa$ alloy [53] (open magenta circles) and our measurements in a Ni-rich $Ni_{60}Mn_{13}Ga_{27}$ alloy (closed red circles) in the martensitic phase with the theoretically calculated spectra for the stoichiometric (full blue curve), Ni-rich $Ni_{56}Mn_{19}Ga_{25}$ (dashed black curve), and $Ni_{62}Mn_{13}Ga_{25}$ (dotted magenta curve) alloys of the $Immm$ orthorhombic structure. The theory well describes the energy position of the major energy peaks for stoichiometric $Ni_2MnGa$ alloy. The theory also correctly describes the major tendency of Ni doping. The excess of Ni atoms modify the electronic structure of the martensitic alloy, resulting in the sharp increase of the low energy peak at 1.7 eV (compare the $\sigma_{1xx}$ experimental spectra for the $Ni_{50}Mn_{25}Ga_{25}$ and $Ni_{60}Mn_{13}Ga_{27}$ compositions in the lower panel of Fig. 4). Such behavior can be explained by the peculiarities of the band structure of $Ni_2MnGa$. The energy bands in the close vicinity of the Fermi energy ($\pm 1$ eV) have predominantly Ni $3d$ character (see Fig. 3). Therefore, with increasing of the Ni content one would expect the increase of the optical absorption in the 0–2 eV region.

Let us now consider the magneto-optical Kerr effect spectra. The comparison of the calculated and experimentally measured Kerr rotation spectra is not a simple task because the measurements have been done in different conditions and for samples with different stoichiometry. Kudryavtsev *et al.* [52–54] measured the MO Kerr effect in a stoichiometric polycrystalline $Ni_2MnGa$ alloy but only in the equatorial geometry which is very sensitive to the angle of incidence. Beran *et al.* [57] studied the polar Kerr effect in a single crystal of Mn-rich off-stoichiometrical $Ni_{50.1}Mn_{28.4}Ga_{21.5}$ alloy during its transformation from the martensitic to austenitic phase in the temperature range from 297 to 373 K in the photon energy range from 1.2 to 5.0 eV (the $T_M$ is equal to 318 K during cooling and 335 K during heating back to austenite in these sample). Our measurements of polar Kerr spectra were carried out for a Ni-rich polycrystalline $Ni_{60}Mn_{13}Ga_{27}$ magnetic shape memory alloy in the martensitic phase in 0.8 to 5.8 eV energy range. It is important to note that the electronic and magnetic properties of Ni-Mn-Ga alloys are more sensitive to the dope composition than to the crystal structure. For example, according to the measurements of Jiang *et al.* [42] the saturation magnetization is equal to 4.38 $\mu_B$ and 2.93 $\mu_B$ in $Ni_{50}Mn_{25}Ga_{25}$ and $Ni_{50}Mn_{30}Ga_{20}$ alloys, respectively. The martensitic transformation temperature $T_M$ is increased from 202 K to 315 K and 350 K if the composition is changed from the stoichiometric one to $Ni_{54}Mn_{21}Ga_{25}$ and $Ni_{50}Mn_{28}Ga_{22}$, respectively. [41] In our calculations we keep the composition to the experimental conditions as close as possible.

The experimental MOKE spectra of the $Ni_{60}Mn_{13}Ga_{27}$ alloy measured in the magnetic field of 1.5 T (open magenta circles in the lower panel of Fig. 5) are compared with the

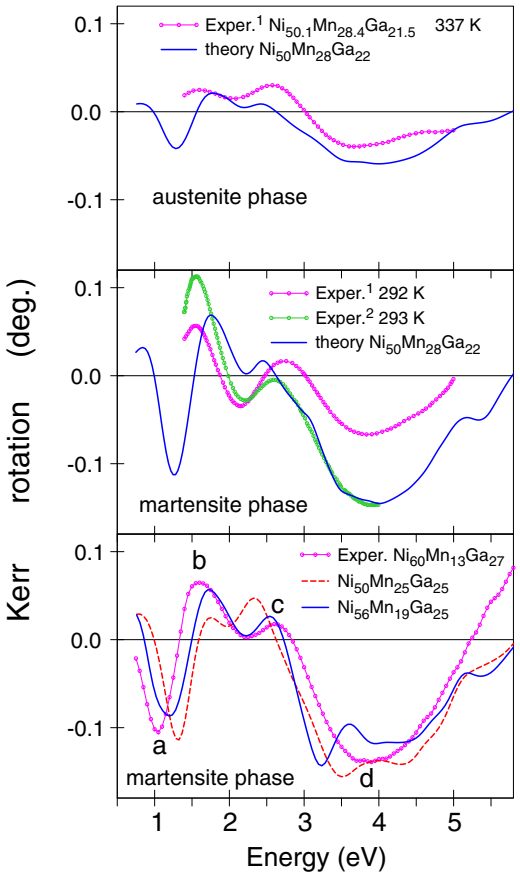


FIG. 5. Upper panel: comparison between the experimental Kerr rotation spectrum [57] of $Ni_{50.1}Mn_{28.4}Ga_{21.5}$ in the austenitic phase at 337 K (open magenta circles) and the calculated spectrum for the cubic $Fm\bar{3}m$ structure (full blue line) of $Ni_{50}Mn_{28}Ga_{22}$ composition. Middle panel: experimental Kerr rotation spectra [Ref. [57] (open magenta circles) and Ref. [56] (open green circles)] of $Ni_{50.1}Mn_{28.4}Ga_{21.5}$ in the martensitic phase in comparison with the calculated spectrum (full blue line) of $Ni_{50}Mn_{28}Ga_{22}$ composition. Lower panel: the experimental Kerr rotation spectrum of $Ni_{60}Mn_{13}Ga_{27}$ alloy in the martensitic phase (open magenta circles) in comparison with the calculated spectrum for the orthorhombic structure with $Ni_2MnGa$ and $Ni_{56}Mn_{19}Ga_{25}$ compositions (dashed red line and full blue line, respectively).

corresponding theoretically calculated spectra in the GGA approximation for $Ni_2MnGa$ and $Ni_{56}Mn_{19}Ga_{25}$ alloys (dashed red line and full blue line, respectively) in Fig. 5. The characteristic features of the measured $Ni_2MnGa$ Kerr rotation spectrum are a sharp negative minimum $a$ in the ir spectral range at $\sim$1.0 eV, two prominent positive peaks $b$ and $c$ at around 1.6 and 2.7 eV with a local minimum in between at 2.2 eV, and a broad negative minimum $d$ in the uv range at 3.8 eV. The essential points of experimental Kerr ellipticity spectrum (not shown) are zero crossings at 1.6 eV and around 3.8 eV (that correspond to the peaks $b$ and $d$ in the Kerr rotation) with a broad positive structure between them and a prominent negative minimum at the energy of $\sim$1.3 eV.

The GGA theoretical calculations for stoichiometric $Ni_2MnGa$ reproduce all the main features ($a$ to $d$), however, the theoretical spectrum is narrower than the experimentally

measured one with the peaks $a$ and $b$ shifted towards higher energy and the peak $c$ shifted in the opposite direction. Besides, the relative intensities of $b$ and $c$ have opposite behavior in comparison with the experimental measurements. This disagreement is partly due to the nonstoichiometry composition of the alloy used in the experimental measurements ($Ni_{60}Mn_{13}Ga_{27}$). The theoretically calculated Kerr spectrum for the $Ni_{56}Mn_{19}Ga_{25}$ composition (full blue curve in the lower panel of Fig. 5) shows much better agreement with the experimental spectrum in the energy position of the $a$ and $b$ peaks as well as the relative intensity of the $b$ and $c$ peaks.

The temperature dependence of the polar Kerr spectrum in a Mn-rich $Ni_{50.1}Mn_{28.4}Ga_{21.5}$ alloy is presented in Fig. 5 [57]. The changes in magneto-optical Kerr spectra with increasing temperature are clearly visible during the martensitic transformation. Comparing the experimentally measured Kerr spectrum in martensitic (middle panel) and austenitic (upper panel) phases we can conclude that the relative intensities of the two prominent peaks $b$ at 1.6 eV and $c$ at 2.8 eV are changed. Besides, the local minimum between these two peaks changes the sign. However, there is no shift of the main features in polar Kerr rotation spectra during the martensitic transformation. We present also the calculated MO Kerr rotation spectra for the low-temperature orthorhombic structure (full blue curve in the middle panel) and the cubic $Fm\bar{3}m$ high-temperature phase (full blue curve in upper panel) of $Ni_{50}Mn_{28}Ga_{22}$ composition. After the transformation, the amplitude of experimentally measured polar Kerr rotation is decreasing with increasing temperature, which can be explained as a gradual loss of magnetization when approaching the ferromagnetic Curie temperature $T_C = 373$ K. Experimentally, a reduction of the saturation magnetization by 40% has been observed when the temperature is raised closer to the Curie temperature. [57] Therefore, to compare with the experimental austenite spectrum we multiply the theoretically calculated spectrum in the upper panel of Fig. 5 by factor 0.6. The theory reproduces well the shape and energy position of the major peaks for the martensitic and austenitic phases and qualitatively describes the change of the relative intensities of $b$ and $c$ peaks during the phase transformation. It is interesting to note that our calculations for the Mn-rich martensitic phase agree even better with earlier measurements by the same authors [56] for the same sample (green empty circles in the middle panel of Fig. 5) than with the later measurements [57] (magenta empty circles in middle panel of Fig. 5), especially for the high energy minimum $d$ at 4 eV.

The interpretation of the MOKE spectra in terms of electronic transitions is a nontrivial task because the complex Kerr rotation is a rather complicated function of both the diagonal and off-diagonal components of the optical conductivity tensor [Eq. (3)]. The off-diagonal part of the conductivity tensor of Ni-rich $Ni_{60}Mn_{13}Ga_{27}$ alloy obtained from experimental MOKE spectra and the complex index of refraction ($n$ and $k$) determined from the ellipsometry measurements are presented in Fig. 6. The theory reproduces all peculiarities of the experimental off-diagonal optical conductivity spectra. In particular, the energy position and the magnitude of the negative peak at 2.2 eV in the $\omega\sigma_{2xy}(\omega)$ spectrum and the positive structure at 1.9 eV in the $\omega\sigma_{1xy}(\omega)$ spectrum are very well reproduced. However, the theoretically calculated

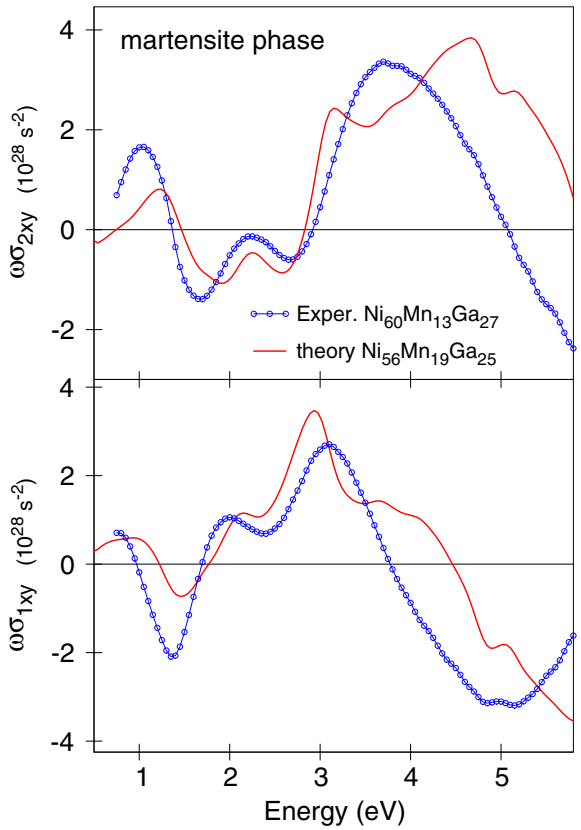


FIG. 6. Comparison between the experimental off-diagonal optical conductivity $\omega\sigma_{xy}$ spectra (blue open circles) of $Ni_{60}Mn_{13}Ga_{27}$ alloy in the martensitic phase and the calculated spectra for the orthorhombic structure with $Ni_{56}Mn_{19}Ga_{25}$ composition (full red lines).

spectrum is narrower than the experimentally measured one in the 0.5 to 3.5 eV range. Besides, the high energy minimum at 5 eV has a blue shift in the $\omega\sigma_{1xy}$ spectrum.

### C. The band-by-band decomposition and the k-space decomposition

To identify the electronic interband transitions responsible for the MO Kerr effects, the analysis of the spectral dependence of the optical conductivity tensor should be performed. The absorptive part of the diagonal optical conductivity tensor element, $\sigma_{1xx}$, and of the off-diagonal part, $\sigma_{2xy}$, are directly connected via Eq. (4) to the microscopic interband optical transitions.

As the absorptive parts of the optical conductivity are additive quantities, to explain the microscopic origin of the MOKE activity of $Ni_2MnGa$ in terms of individual electronic transitions we performed the decomposition of the calculated $\sigma_{1xx}$ and $\sigma_{2xy}$ spectra into the contributions arising from separate interband transitions

Although the experimental MOKE spectra of $Ni_2MnGa$ alloy change through the martensitic transition at $T_M$ and their shape is strongly affected by the alloy composition, the characteristic features of the measured Kerr rotation spectrum are the same (Fig. 5) with a sharp negative minimum $a$ at $\sim$1.0 eV, two prominent positive peaks $b$ and $c$ at around

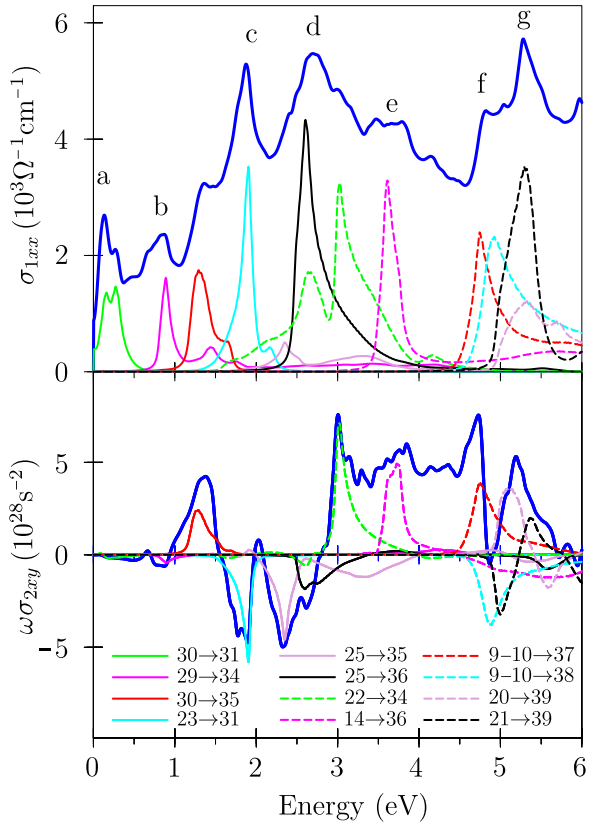


FIG. 7. Contributions of different interband transitions to the diagonal $\sigma_{1xx}$ and off-diagonal $\sigma_{2xy}$ spectra (thick solid lines) of $Ni_2MnGa$.

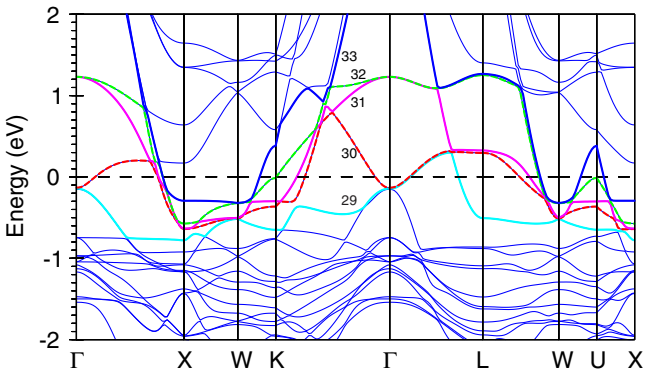


FIG. 8. Fully relativistic spin-polarized GGA energy band structure of $Ni_2MnGa$ near the Fermi level.

1.6 and 2.7 eV and a broad negative minimum $d$ at 3.8 eV. Therefore we perform the band-by-band and the **k**-space decomposition of the MOKE spectra for the cubic austenitic phase (Fig. 7). We also neglect the intraband contributions for simplicity.

In spin-polarized band structure calculations three majority-spin bands (17 to 19) and two minority-spin bands (13 and 14) cross the Fermi level. In spin-polarized fully-relativistic calculations the spin-orbit interaction mixes spin-up and -down bands and the numeration of the energy bands is changed. In the last case five energy bands with numbers from 29 to 33 cross the Fermi level. Figure 8 presents the energy bands of $Ni_2MnGa$ alloy in the close vicinity of the Fermi level.

Strong interband absorption occurs at 0.3 and 0.8 eV (peaks $a$ and $b$), and sharp structures appear at 1.90, 2.4, and 5.4 eV (peaks $c$, $d$, and $g$). Broad peaks located at 3.7 and 5.0 eV ($e$ and $f$) can also be selected. The characteristic for the $Ni_2MnGa$ intensive peak in $\sigma_{1xx}$ around 0.3 eV is mainly determined by $30 \rightarrow 31$ interband transitions (Fig. 7). These transitions occur mostly at the $L - W$ symmetry direction (see Fig. 8). The corresponding peak $b$ is mostly derived from the $29 \rightarrow 34$ transitions in the close vicinity of the Fermi level. These two peaks $a$ and $b$ are hard to separate from strong intraband Drude-like transitions presented in the experimentally measured OC spectrum (Fig. 4). The next peaks $c$ and $d$ arise from the $23 \rightarrow 31$ (peak $c$) and $25 \rightarrow 36$, $22 \rightarrow 34$ (peak $d$) transitions. The peak $g$ with the low energy shoulder $f$ is mostly determined by the interband transitions $20,21 \rightarrow 39$ and $9,10 \rightarrow 37,38$. The shoulder $e$ is formed by the $14 \rightarrow 36$ interband transitions.

The characteristic features of $\sigma_{2xy}$ of $Ni_2MnGa$ are a positive peak at 1.3 eV, negative structures at around 1.8 and 2.3 eV, an intensive wide structure with three maxima in the 2.9 to 4.9 eV energy range and a strong single positive peak at 5.2 eV. The interband transitions $30 \rightarrow 31$ and $29 \rightarrow 34$ which form the ir $a$ and $b$ peaks in the diagonal OC spectrum $\sigma_{1xx}$ are almost invisible in the off-diagonal OC $\sigma_{2xy}$ (Fig. 7). Two negative peaks at 1.8 and 2.3 eV are determined by the $23 \rightarrow 31$ and $25 \rightarrow 35$ transitions, respectively. The intensive wide structure with three maxima in the 2.9–4.9 eV range arises mostly from the $22 \rightarrow 34$, $14 \rightarrow 36$ and $9,10 \rightarrow 37,38$ transitions.

We can conclude that while the high energy uv part of both the diagonal and off-diagonal OC are formed by the same sets of interband transitions, different transitions are responsible for the low energy ir part of the $\sigma_{1xx}$ and $\sigma_{2xy}$ spectra.

To see how the interband transitions between individual bands are located in the reciprocal space of $Ni_2MnGa$ we performed the **k**-space decomposition of the interband transitions into transitions occurring in the vicinity of the high symmetry points and symmetry directions of the Brillouin zone. For this aim we summed all the transitions between bands $n$ and $m$ in a cubic volume surrounding a given point with a cube edge equal to 0.125 of the $\Gamma - X$ distance (it contains approximately 1.5% of the whole BZ volume). Although the results depend on the volume of the cube, one can identify the transitions essentially with these points and their nearest neighborhood.

Figure 9 illustrates the results of the decomposition. As we already mentioned above, the ir peak $a$ around 0.3 eV in the $\sigma_{1xx}$ spectrum is mainly determined by the $30 \rightarrow 31$ interband transitions which take place from regions in the $L - W$ symmetry direction near $E_F$ in the BZ (see Fig. 8) while, in formation of the other transitions, quite a large volume of the Brillouin zone has to be taken into account. The most intense interband transitions in both the diagonal and off-diagonal optical conductivity arise from the same parts of the BZ located near the $U$ symmetry point and along the $U - L$ symmetry direction. These transitions almost completely describe the MO response in $Ni_2MnGa$. On the other hand, there are additional contributions in the case of the diagonal optical conductivity $\sigma_{1xx}$ spectrum coming from

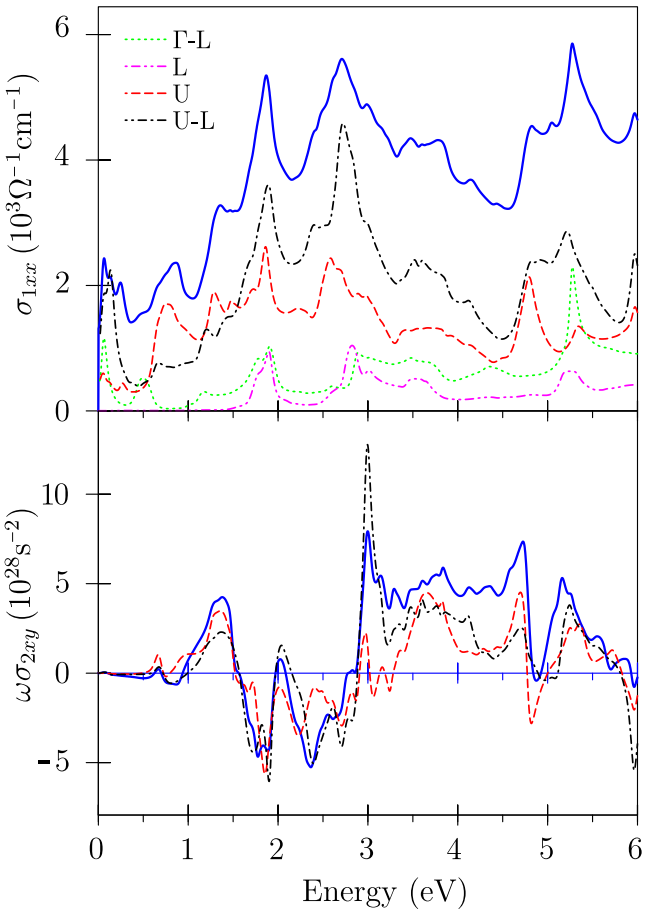


FIG. 9. Decomposition of the $\sigma_{1xx}$ and $\sigma_{2xy}$ $n \to m$ interband transitions in $Ni_2MnGa$ alloy into transitions localized around different symmetry points and symmetry directions in the BZ.

the $\Gamma - L$ symmetry direction and from the vicinity of the $L$ symmetry point.

## IV. SUMMARY

The polar MOKE spectra of a polycrystalline sample of the Ni-Mn-Ga alloy of $Ni_{60}Mn_{13}Ga_{27}$ composition were measured by means of the polarization modulation method over the photon energy range $0.8 \leqslant h\nu \leqslant 5.8$ eV in magnetic field up to 1.5 T. The optical properties (refractive index $n$ and extinction coefficient $k$) were measured directly by spectroscopic ellipsometry using the rotating analyzer method.

The electronic structure of $Ni_2MnGa$ Heusler alloy for the cubic austenitic and modulated 7M-like incommensurate martensitic phases were investigated theoretically from first principles, using the fully relativistic Dirac LMTO band structure method. The equilibrium crystal structures calculations with the exchange-correlation potential of GGA type in the PBE version agree extremely well with the relevant experimental data for both the austenite and the martensite 7M modulated structures. It is found that the calculated total magnetic moments and Curie temperature are in accordance with the experiment as well.

The *ab initio* LMTO calculations reproduce well the experimental MOKE spectra of $Ni_2MnGa$ alloy and allow us to explain the microscopic origin of the MO response in terms of interband transitions. The band-by-band and the **k**-space decomposition of the $Ni_2MnGa$ MO spectra have been performed and the transitions responsible for the prominent structures in the spectra identified. The most intense interband transitions in both the diagonal and off-diagonal optical conductivity arise from the same parts of the BZ located near the $U$ symmetry point and along the $U - L$ symmetry direction. These transitions almost completely describe the MO response in $Ni_2MnGa$. On the other hand, there are additional contributions in the case of the diagonal optical conductivity $\sigma_{1xx}$ spectrum coming from the $\Gamma - L$ symmetry direction and from the vicinity of the $L$ symmetry point.

The characteristic features of the measured $Ni_2MnGa$ Kerr rotation spectrum are a sharp negative minimum at ∼1.0 eV, two prominent positive peaks at around 1.6 and 2.7 eV, with a local minimum in between at 2.2 eV, and a broad negative minimum in the uv range at 3.8 eV. We found that the optical and MOKE properties of Ni-Mn-Ga systems are very sensitive to the deviation from the stoichiometric composition, resulting in different energy position and relative intensities of the prominent features. The theory reproduces well the shape and energy position of the major peaks for MOKE spectra in the martensitic and austenitic phases and qualitatively describes the change of the relative intensities of the spectral peaks during the martensitic phase transformation.

One of the main results of our study is that the computational material design of Ni-Mn-Ga Heusler alloys is possible. Comparing our current MOKE measurements and experiments of other groups with our first-principles simulations we found a robust methodology to describe adequately structural, electronic, magnetic, optical, and magneto-optical properties of these Heusler compounds. Probing various functionals within the modern density functional theory we have shown that all the above mentioned properties could be correctly obtained with a conventional GGA approach. Using this framework we could make reliable predictions for further alloy compositions under various martensitic transformations, some of which were even not yet accessible with experiments. Summarizing, our finding provides a solid background to study ferromagnetic shape-memory Ni-Mn-Ga alloys and opens possibilities in computational material design of these materials. The next ambitious goal of our research is to understand the microscopic origin of the martensitic phase transitions in these compounds for various chemical compositions.

## ACKNOWLEDGMENTS

V. N. Antonov gratefully acknowledges the hospitality at Bialystok University during his stay. We are very much indebted to Dr. Alexander Yaresko for his contribution in successful implementation of GGA approach in the relativistic LMTO code. Authors would like to thank Prof. T. Breczko for providing samples for the measurements of the optical and MO Kerr spectra. This work was supported by Science and Technology Center in Ukraine STCU, Project No. 6255. This work also was partially funded by the Joint Initiative for Research and Innovation within the Fraunhofer and Max Planck cooperation program.

[1] Y. Ma, S. Awaji, M. Watanabe, M. Matsumoto, and N. Kobayashi, Solid State Commun. **113**, 671 (2000).

[2] P. J. Webster, K. R. A. Ziebeck, S. L. Town, and M. S. Peak, Philos. Mag. B **49**, 295 (1984).

[3] K. Ullakko, J. K. Huang, C. Kantner, R. C. O'Handley, and V. V. Kokorin, Appl. Phys. Lett. **69**, 1966 (1996).

[4] S. J. Murray, M. Marioni, S. M. Allen, R. C. O'Handley, and T. A. Lograsso, Appl. Phys. Lett. **77**, 886 (2000).

[5] A. Sozinov, A. A. Likhachev, N. Lanska, and K. Ullakko, Appl. Phys. Lett. **80**, 1746 (2002).

[6] F.-X. Hu, B.-G. Shen, J.-R. Sun, and G.-H. Wu, Phys. Rev. B **64**, 132412 (2001).

[7] C. Biswas, R. Rawat, and S. R. Barman, Appl. Phys. Lett. **86**, 202508 (2005).

[8] S. Fujii, S. Ishida, and S. Asano, J. Phys. Soc. Jpn. **58**, 3657 (1989).

[9] A. Ayuela, J. Enkovaara, K. Ullakko, and R. Nieminen, J. Phys. Condens. Matter **11**, 2017 (1999).

[10] M. Pugaczowa-Michalska, Acta Phys. Pol. A **96**, 467 (1999).

[11] O. I. Velikokhatnyi and I. I. Naumov, Phys. Solid State **41**, 617 (1999).

[12] V. V. Godlevsky and K. M. Rabe, Phys. Rev. B **63**, 134407 (2001).

[13] A. Ayuela, J. Enkovaara, and R. M. Nieminen, J. Phys. Condens. Matter **14**, 5325 (2002).

[14] J. Enkovaara, A. Ayuela, L. Nordstrom, and R. M. Nieminen, J. Appl. Phys. **91**, 7798 (2002).

[15] J. Enkovaara, A. Ayuela, L. Nordstrom, and R. M. Nieminen, Phys. Rev. B **65**, 134422 (2002).

[16] Y. Lee, J. Y. Rhee, and B. N. Harmon, Phys. Rev. B **66**, 054424 (2002).

[17] A. T. Zayak, P. Entel, J. Enkovaara, A. Ayuela, and R. M. Nieminen, Phys. Rev. B **68**, 132402 (2003).

[18] J. Enkovaara, A. Ayuela, J. Jalkanen, L. Nordström, and R. M. Nieminen, Phys. Rev. B **67**, 054417 (2003).

[19] S. Kulkova, S. Eremeev, and S. Kulkov, Solid State Commun. **130**, 793 (2004).

[20] S. R. Barman, S. Banik, and A. Chakrabarti, Phys. Rev. B **72**, 184410 (2005).

[21] A. Chakrabarti, C. Biswas, S. Banik, R. S. Dhaka, A. K. Shukla, and S. R. Barman, Phys. Rev. B **72**, 073103 (2005).

[22] G. D. Liu, X. F. Dai, S. Y. Yu, Z. Y. Zhu, J. L. Chen, G. H. Wu, H. Zhu, and J. Q. Xiao, Phys. Rev. B **74**, 054435 (2006).

[23] S. Banik, A. Chakrabarti, U. Kumar, P. K. Mukhopadhyay, A. M. Awasthi, R. Ranjan, J. Schneider, B. L. Ahuja, and S. R. Barman, Phys. Rev. B **74**, 085110 (2006).

[24] S. Banik, R. Ranjan, A. Chakrabarti, S. Bhardwaj, N. P. Lalla, A. M. Awasthi, V. Sathe, D. M. Phase, P. K. Mukhopadhyay, D. Pandey *et al.*, Phys. Rev. B **75**, 104107 (2007).

[25] C. Jie, L. Yan, S. Jia-Xiang, and X. Hui-Bin, Chin. Phys. Lett. **26**, 047101 (2009).

[26] R. Ranjan, S. Singh, H. Boysen, D. Trots, S. Banik, A. M. Awasthi, P. K. Mukhopadhyay, and S. R. Barman, J. Appl. Phys. **106**, 033510 (2009).

[27] Q.-M. Hu, C.-M. Li, R. Yang, S. E. Kulkova, D. I. Bazhanov, B. Johansson, and L. Vitos, Phys. Rev. B **79**, 144112 (2009).

[28] C.-M. Li, H.-B. Luo, Q.-M. Hu, R. Yang, B. Johansson, and L. Vitos, Phys. Rev. B **82**, 024201 (2010).

[29] J. Bai, J. M. Raulot, Y. D. Zhang, C. Esling, X. Zhao, and L. Zuo, J. Appl. Phys. **108**, 064904 (2010).

[30] J. Bai, J. M. Raulot, Y. D. Zhang, C. Esling, X. Zhao, and L. Zuo, J. Appl. Phys. **109**, 014908 (2011).

[31] Y. Qawasmeh and B. Hamad, J. Appl. Phys. **111**, 033905 (2012).

[32] M. B. Sahariah, S. Ghosh, C. S. Singh, S. Gowtham, and R. Pandey, J. Phys. Condens. Matter **25**, 025502 (2013).

[33] A. Chakrabarti, M. Siewert, T. Roy, K. Mondal, A. Banerjee, M. E. Gruner, and P. Entel, Phys. Rev. B **88**, 174116 (2013).

[34] T. Roy, M. E. Gruner, P. Entel, and A. Chakrabarti, J. Alloys Comp. **632**, 822 (2015).

[35] Y. Polyak, V. Drchal, J. Kudrnovsky, O. Heczko, J. Honolka, V. Chab, J. Kopecek, and J. Lancok, Phys. Rev. B **91**, 165115 (2015).

[36] N. Xu, J. M. Raulot, Z. B. Li, J. Bai, B. Yang, Y. D. Zhang, X. Y. Meng, X. Zhao, L. Zuo, and C. Esling, J. Mater. Sci. **50**, 3825 (2015).

[37] W. H. Wang, F. X. Hu, J. L. Chen, Y. X. L. Z. Wang, and G. H. Wu, IEEE Trans. Magn. **37**, 2715 (2001).

[38] I. Karaman, H. E. Karaca, B. Basaran, D. C. Lagoudas, Y. I. Chumlyakov, and H. J. Maier, Scr. Mater. **55**, 403 (2006).

[39] H. E. Karaca, I. Karaman, B. Basaran, D. C. Lagoudas, Y. I. Chumlyakov, and H. J. Maier, Acta Mater. **55**, 4253 (2007).

[40] G.-H. Yu, Y.-L. Xu, Z.-H. Liu, H.-M. Qiu, Z.-Y. Zhu, X.-P. Huang, and L.-Q. Pan, Rare Met. **34**, 527 (2015).

[41] B. Dutta, A. Cakir, C. Giacobbe, A. Al-Zubi, T. Hickel, M. Acet, and J. Neugebauer, Phys. Rev. Lett. **116**, 025503 (2016).

[42] C. Jiang, Y. Muhammad, L. Deng, W. Wu, and H. Xu, Acta Mater. **52**, 2779 (2004).

[43] A. Zheludev, S. M. Shapiro, P. Wochner, A. Schwartz, M. Wall, and L. E. Tanner, Phys. Rev. B **51**, 11310 (1995).

[44] S. M. Shapiro, P. Vorderwisch, K. Habicht, K. Hradil, and H. Schneider, Europhys. Lett. **77**, 56004 (2007).

[45] S. W. D'Souza, A. Rai, J. Nayak, M. Maniraj, R. S. Dhaka, S. R. Barman, D. L. Schlagel, T. A. Lograsso, and A. Chakrabarti, Phys. Rev. B **85**, 085123 (2012).

[46] L. Uba, S. Uba, O. Horpynyuk, V. N. Antonov, and A. N. Yaresko, J. Appl. Phys. **91**, 775 (2002).

[47] V. N. Antonov, M. Galli, F. Marabelli, A. N. Yaresko, A. Y. Perlov, and E. Bauer, Phys. Rev. B **62**, 1742 (2000).

[48] M. Veis, M. Zahradnik, R. Antos, S. Visnovsky, P. Lecoeur, D. Esteve, S. Autier-Laurent, J.-P. Renard, and P. Beauvillain, Sci. Technol. Adv. Mater. **15**, 015001 (2014).

[49] M. Veis, S. Visnovsky, P. Lecoeur, A.-M. Haghiri-Gosnet, J.-P. Renard, P. Beauvillain, W. Prellier, B. Mercey, J. Mistrik, and T. Yamaguchi, J. Phys. D: Appl. Phys. **42**, 195002 (2009).

[50] L. Uba, S. Uba, V. N. Antonov, A. N. Yaresko, T. Slezak, and J. Korecki, Phys. Rev. B **62**, 13731 (2000).

[51] J. F. Wan and J. N. Wang, Physica B **355**, 172 (2005).

[52] Y. Zhou, H. Xu, X. Jin, Y. V. Kudryavtsev, Y. P. Lee, and K. W. Kim, J. Korean Phys. Soc. **39**, 698 (2001).

[53] Y. V. Kudryavtsev, Y. P. Lee, and J. Y. Rhee, Phys. Rev. B **66**, 115114 (2002).

[54] N. Lee, B. J. Kim, M. D. Huang, Y. P. Lee, J. Y. Rhee, and Y. V. Kudryavtsev, J. Korean Phys. Soc. **45**, 34 (2004).

[55] J. mok Park, Ph.D. thesis, Iowa State University, Ames, 2004.

[56] M. Veis, L. Beran, M. Zahradnik, R. Antos, L. Straka, J. Kopecek, and L. Fekete, J. Appl. Phys. **115**, 17A936 (2014).

[57] L. Beran, P. Cejpek, M. Kulda, R. Antos, V. Holy, M. Veis, L. Straka, and O. Heczko, J. Appl. Phys. **117**, 17A919 (2015).

[58] S. Singh, V. Petricek, P. Rajput, A. H. Hill, E. Suard, S. R. Barman, and D. Pandey, Phys. Rev. B **90**, 014109 (2014).
[59] S. Singh, J. Bednarcik, S. R. Barman, C. Felser, and D. Pandey, Phys. Rev. B **92**, 054112 (2015).
[60] P. J. Brown, J. Crangle, T. Kanomata, M. Matsumoto, K.-U. Neumann, B. Ouladdiaf, and K. R. A. Ziebeck, J. Phys. Condens. Matter **14**, 10159 (2002).
[61] V. V. Martynov, J. Phys. IV (France) **05**, C8-91 (1995).
[62] R. Ranjan, S. Banik, S. R. Barman, U. Kumar, P. K. Mukhopadhyay, and D. Pandey, Phys. Rev. B **74**, 224443 (2006).
[63] L. Righi, F. Albertini, G. Calestani, L. Pareti, A. Paoluzi, C. Ritter, P. A. Algarabel, L. Morellon, and M. R. Ibarra, Solid State Chem. **179**, 3525 (2006).
[64] T. Fukuda, H. Kushida, M. Todai, T. Kakeshita, and H. Mori, Scr. Mater. **61**, 473 (2009).
[65] M. Belesi, L. Giebeler, C. G. F. Blum, U. K. Rossler, B. Buchner, and S. Wurmehl, Phys. Rev. B **91**, 134415 (2015).
[66] W. H. Kleiner, Phys. Rev. **142**, 318 (1966).
[67] F. J. Kahn, P. S. Pershan, and J. P. Remeika, Phys. Rev. **186**, 891 (1969).
[68] S. Visnovsky, Czech. J. Phys. B **34**, 969 (1984).
[69] J. Schoenes, in *Electronic and Magnetic Properties of Metals and Ceramics*, edited by R. W. Cahn, P. Haasen, and E. J. Kramer (Verlag Chemie, Weinheim, 1992), Vol. 3A of Materials Science and Technology, p. 147, volume editor: K. H. J. Buschow.
[70] R. Kubo, J. Phys. Soc. Jpn. **12**, 570 (1957).
[71] C. S. Wang and J. Callaway, Phys. Rev. B **9**, 4897 (1974).
[72] V. N. Antonov, A. I. Bagljuk, A. Y. Perlov, V. V. Nemoshkalenko, V. N. Antonov, O. K. Andersen, and O. Jepsen, Fizika Nizkikh Temperatur **19**, 689 (1993).
[73] L. Uba, S. Uba, V. N. Antonov, A. N. Yaresko, and R. Gontarz, Phys. Rev. B **64**, 125105 (2001).
[74] V. N. Antonov, L. Uba, S. Uba, A. N. Yaresko, A. Y. Perlov, and V. V. Nemoshkalenko, Low Temp. Phys. **27**, 425 (2001).
[75] O. K. Andersen, Phys. Rev. B **12**, 3060 (1975).
[76] V. V. Nemoshkalenko, A. E. Krasovskii, V. N. Antonov, V. N. Antonov, U. Fleck, H. Wonn, and P. Ziesche, Phys. status solidi B **120**, 283 (1983).
[77] J. P. Perdew, K. Burke, and M. Ernzerhof, Phys. Rev. Lett. **77**, 3865 (1996).
[78] J. P. Perdew, K. Burke, and M. Ernzerhof, Phys. Rev. Lett. **78**, 1396 (1997).
[79] P. E. Blöchl, O. Jepsen, and O. K. Andersen, Phys. Rev. B **49**, 16223 (1994).
[80] A. I. Liechtenstein, M. I. Katsnelson, V. P. Antropov, and V. A. Gubanov, J. Magn. Magn. Mater. **67**, 65 (1987).
[81] S. Tyablikov, *Methods in the Quantum Theory of Magnetism* (Plenum Press, New York, 1967).
[82] V. I. Anisimov, J. Zaanen, and O. K. Andersen, Phys. Rev. B **44**, 943 (1991).
[83] V. V. Khovailo, V. Novosad, T. Takagi, D. A. Filippov, R. Z. Levitin, and A. N. Vasiljev, Phys. Rev. B **70**, 174413 (2004).